Anti-amyloid treatment is broadly effective in neuronopathic mucopolysaccharidoses and synergizes with gene therapy in MPS-IIIA

Marianna Giaccio,[1] Antonio Monaco,[1] Laura Galiano,[1] Andrea Parente,[1,2] Luigi Borzacchiello,[1,2] Riccardo Rubino,[1] Frank-Gerrit Klärner,[3] Dennis Killa,[3] Claudia Perna,[4] Pasquale Piccolo,[4] Marcello Marotta,[8] Xuefang Pan,[5] Marie Khijniak,[6] Ibrar Siddique,[6] Thomas Schrader,[3] Alexey V. Pshezhetsky,[5] Nicolina Cristina Sorrentino,[4,8] Gal Bitan,[6,7] and Alessandro Fraldi[1,8]

[1]CEINGE-Biotecnologie Avanzate Franco Salvatore, Via G. Salvatore, 486 Napoli, Italy; [2]Dipartimento di Scienze Mediche Traslazionali, Università Degli Studi di Napoli "Federico II" Via S. Pansini, 5, Napoli, Italy; [3]Department of Chemistry, University of Duisburg-Essen, Universitaetsstrasse 7, 45117 Essen, Germany; [4]Telethon Institute of Genetics and Medicine (TIGEM), Via C. Flegrei, 34, Pozzuoli, Napoli, Italy; [5]Department of Pediatrics, Centre Hospitalier Universitaire Sainte-Justine Research Center, University of Montreal, Montreal, QC, Canada; [6]Department of Neurology, David Geffen School of Medicine, University of California, Los Angeles, Los Angeles, CA, USA; [7]Brain Research Institute and Molecular Biology Institute, University of California, Los Angeles, Los Angeles, CA, USA; [8]Dipartimento di Medicina Clinica e Chirurgia, Università Degli Studi di Napoli "Federico II" Via S. Pansini, 5, Napoli, Italy

Mucopolysaccharidoses (MPSs) are childhood diseases caused by inherited deficiencies in glycosaminoglycan degradation. Most MPSs involve neurodegeneration, which to date is untreatable. Currently, most therapeutic strategies aim at correcting the primary genetic defect. Among these strategies, gene therapy has shown great potential, although its clinical application is challenging. We have shown previously in an MPS-IIIA mouse model that the molecular tweezer (MT) CLR01, a potent, broad-spectrum anti-amyloid small molecule, inhibits secondary amyloid storage, facilitates amyloid clearance, and protects against neurodegeneration. Here, we demonstrate that combining CLR01 with adeno-associated virus (AAV)-mediated gene therapy, targeting both the primary and secondary pathologic storage in MPS-IIIA mice, results in a synergistic effect that improves multiple therapeutic outcomes compared to each monotherapy. Moreover, we demonstrate that CLR01 is effective therapeutically in mouse models of other forms of neuronopathic MPS, MPS-I, and MPS-IIIC. These strongly support developing MTs as an effective treatment option for neuronopathic MPSs, both on their own and in combination with gene therapy, to improve therapeutic efficacy and translation into clinical application.

INTRODUCTION

Mucopolysaccharidoses (MPSs) are devastating, progressive, inherited diseases belonging to the large family of lysosomal-storage diseases (LSDs). There are seven types of MPSs: MPS-I, MPS-II, MPS-III, MPS-IV, MPS-VI, MPS-VII, and MPS-IX, each caused by deficiency in lysosomal hydrolases required for the degradation of glycosaminoglycans (GAGs), which consequently accumulate as primary lysosomal storage.[1] MPSs are rare conditions, with an estimated total incidence of ∼1 in 20,000 live births. They affect predominantly children, causing multisystemic clinical manifestations and leading to death, typically by the second decade of life.[1,2] Progressive neurological deterioration is the most prominent clinical feature of MPSs and is characterized by developmental delay, behavioral dysfunctions, and cognitive and motor dysfunctions. Neuronopathy affects most MPS patients, namely MPS-I (Hurler syndrome), MPS-II (Hunter syndrome), MPS-III (Sanfilippo types A, B, C, and D syndromes), and MPS-VII (Sly syndrome), in which degradation of heparan sulfate is impaired. It is therefore the major therapeutic target for these disorders.[1]

As in many other LSDs, impairment of the autophagy-lysosomal pathway (ALP), the major degradation process in the cell, is a key pathophysiological feature of MPSs.[3,4] We and others have shown previously that in several neuronopathic MPSs, impairment of the ALP occurs due to blockage of the autophagy flux.[5–7]

There are no therapies that treat effectively the neurological deficits in patients with MPSs, and developing disease-modifying therapies for these diseases is an urgent, unmet medical need. The vast majority of therapies tested pre-clinically or clinically for MPSs to date have been based on enzyme replacement therapy (ERT), gene therapy, or stem cell-based therapy aimed at correcting the specific hydrolytic lysosomal defects and the primary storage of GAGs by supplying a functional copy of the deficient enzyme or gene.[8–13] However, effective clinical application of these strategies is highly challenging due to the difficulty in achieving and maintaining therapeutic threshold

levels of the corrective enzyme in the target tissues, particularly in the brain, before irreversible neurodegenerative processes take place. High dosage and/or repeated administration of the therapeutic enzymes/viral vectors are not only costly but also potentially toxic. Moreover, such therapies must be developed separately for each MPS type.

Adeno-associated virus (AAV)-mediated gene delivery by different administration routes has been explored widely in preclinical models of MPS, and some candidates have reached clinical trials.[8,14,15] Phase 1/2 clinical trials based on AAV9-mediated genes administered intravenously (these trials are registered at ClinicalTrials.gov: NCT02716246, NCT04088734, and NCT03315182) or intrathecally (European Union Drug Regulating Authorities Clinical Trials Database [EudraCT]: 2015-000359-26) are ongoing for MPS-IIIA and -IIIB. Two clinical trials based on intracerebral injection of AAV serotype rh10 already have been completed for MPS-IIIA and -IIIB,[16,17] and two for MPS-IIIA have started more recently (NCT03612869; EudraCT: 2015-000359-26). Trials based on the intrathecal delivery of AAV9 (NCT03580083) or AAV serotype 6-mediated intravenous delivery of zinc-finger nuclease (NCT02702115) are ongoing for MPS-I and MPS-II (NCT03566043).

All these approaches have shown potential benefits in animal models, yet effective application to patients with MPS has encountered substantial obstacles.[13,14,18] The doses of the AAV vectors are a limiting factor for achieving wide CNS distribution and sustained efficacious levels of the therapeutic enzyme. Scaling up these doses for human use has led to toxicity and neutralizing immune responses, especially upon systemic administration.[14,19–21] Importantly, animal studies and clinical trials have shown that treatments based on supplying a functional protein or gene, including AAV-mediated gene therapies, were largely ineffective when applied during late disease stages, highlighting the importance of intervening before extensive neurologic damage occurs.[18] Thus, although therapies targeting the primary lysosomal-storage defect are rational and promising, new strategies are urgently needed to improve the therapeutic efficacy in clinical trials. Here, we tested the hypothesis that combining a corrective gene therapy with targeting the secondary amyloid accumulation downstream of the inherited primary defect could meet this need.

Amyloidogenic proteins, including α-synuclein (α-syn), tau, and amyloid β-protein (Aβ) have been reported to accumulate as secondary storage materials in multiple MPSs. Accumulation of Aβ deposits in patients with MPS-I and -III was first reported 25 years ago.[22] A later report found phosphorylated α-syn aggregates in swollen cortical neurons of patients with MPS-II and -IIIB,[23] and recently, amyloid deposition was found postmortem in the neurons of patients with MPS-I, -II, and -III.[24] Animal studies have provided additional evidence for the accumulation of Aβ, tau, p-tau, prion protein, and α-syn in mouse models of MPS-I,[25] -IIIA,[7,26–29] -IIIB[30–32] and -IIIC.[33] Nonetheless, the neuropathogenic relevance of amyloid accumulation in MPSs has remained largely unexplored and often was regarded as an epiphenomenon.

Recently, we have shown that brain deposition of multiple amyloid proteins was a key contributor to neurodegenerative processes in a mouse model of MPS-IIIA,[34] one of the most common and severe types of neuronopathic MPS, causing impairment of the ALP and severe neuroinflammation.[7,35] Moreover, we found that inhibiting amyloid deposition by treating MPS-IIIA mice with the molecular tweezer (MT) CLR01 dramatically reduced amyloid accumulation in their brains and protected the mice against neurodegeneration, neuroinflammation, and memory loss, providing prolonged relief and considerable delay of disease onset.[7]

MTs act as potent broad-spectrum inhibitors of the self-assembly of amyloidogenic proteins into toxic oligomers and aggregates using unconventional mechanisms based on competing with a combination of hydrophobic and electrostatic interactions that are key to abnormal self-assembly.[36–39] Moreover, MTs rapidly concentrate in lysosomes,[40] exactly where the toxic secondary storage occurs in MPS, and facilitate the degradation of the amyloid proteins in vivo.[34]

Here, we explored further the therapeutic potential of CLR01 for neuronopathic MPSs by (1) testing whether combining CLR01 treatment with AAV9-mediated gene therapy would lead to significant synergy and (2) testing the therapeutic efficacy of CLR01 in additional mouse models of MPS with prominent CNS involvement, namely MPS-I, the most common form of MPS, and MPS-IIIC, another severe neuronopathic form of Sanfilippo syndrome.

Our results indicate that CLR01 is broadly effective against neuronopathic MPS, and its combination with AAV-mediated gene therapy in MPS-IIIA mice results in synergistic, therapeutic effects, positioning the combination therapy as a particularly promising direction for clinical translation.

RESULTS

CLR01 treatment and gene therapy reduce neuroinflammation synergistically in MPS-IIIA mice

AAV-mediated gene therapy, although highly promising for the treatment of neuronopathy in MPSs, has been faced with several challenges when translated to clinical trials, resulting in insufficient therapeutic outcomes. Therefore, we tested whether the therapeutic efficacy of a combination of AAV-mediated gene therapy and CLR01 treatment in MPS-IIIA mice would lead to significant improvement compared to each monotherapy. A proof of efficacy of CLR01 administered subcutaneously (SC) at 1 mg/kg was initially demonstrated in this mouse model.[7] Moreover, a gene therapy protocol based on AAV serotype 9-mediated intracerebroventricular (ICV) administration of the SGSH (N-sulfoglucosamine sulfohydrolase) gene was tested successfully in MPS-IIIA mice at an early disease stage (2 months of age)[41,42] and is now in a clinical trial (EudraCT: 2015-000359-26).

Based on these results, here, we administered AAV9-SGSH (4×10^{12} genome copies [GC]s/kg) ICV to MPS-IIIA mice at 2 months of age followed by 1 mg/kg CLR01 administered SC three times per week
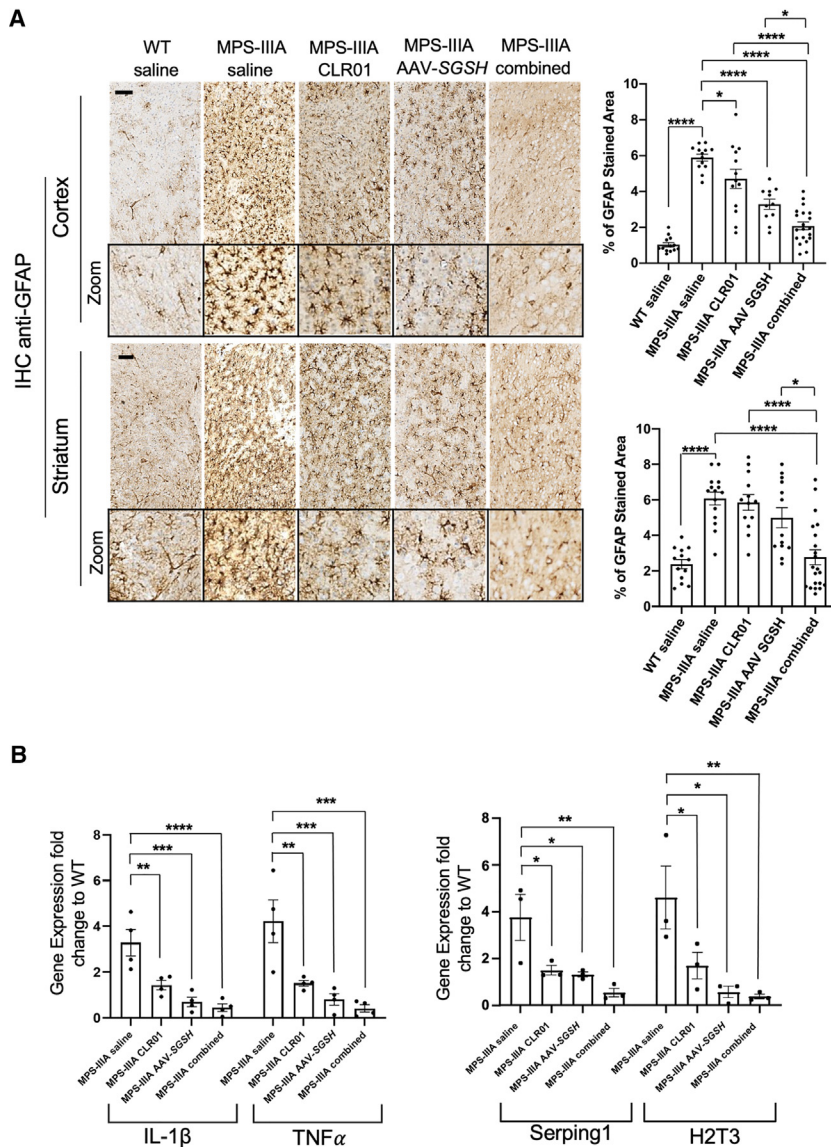
A

Figure 1. Combining CLR01 with AAV gene therapy results in a synergistic effect reducing neuroinflammation

(A) MPS-IIIA mice were treated with 1.0 mg/kg CLR01 SC three times per week starting at 4.5 months of age, 4×10^{12} GCs/kg AAV9-*SGSH* viral vectors ICV at 2 months of age, or with the combination of both treatments. As controls, WT and MPS-IIIA mice were treated with saline. Mice were analyzed at 9 months of age for astrogliosis by IHC using an anti-GFAP antibody on sagittal cortical or striatal sections. Scale bars represent 30 μm. The bar graphs depict the percentage of GFAP$^+$ area quantified in 11–21 different fields (represented by individual dots) from at least three mice in each experimental group. The data are presented as mean ± SEM. (B) Microglial and astroglial activation markers were evaluated by real-time PCR analysis in brain extracts. Gene expression is reported as fold change over WT mice. A total of 3–4 mice (represented by individual dots) in each group were analyzed. The data are presented as mean ± SEM. *$p < 0.05$; **$p < 0.01$; ***$p < 0.001$; ****$p < 0.0001$. $p > 0.05$ are not presented. One-way ANOVA with Tukey's post hoc multiple comparison test.

B

starting at 4.5 months of age (combination therapy group). The combination therapy group was compared to two monotherapy groups: mice injected ICV with 4×10^{12} GCs/kg AAV9-*SGSH* at 2 months of age but not receiving CLR01, or mice injected SC three times per week with 1 mg/kg CLR01 starting at 4.5 months of age without prior administration of the gene therapy. An additional control group included wild-type (WT) and MPS-IIIA mice receiving PBS to provide the full range between healthy mice and mice displaying the full disease phenotype, respectively. All the mice were sacrificed at 9 months of age, and their brains were examined using biochemical and histological assays.

Neuroinflammation is a prominent sign of neuropathology in both patients with neuronopathic MPSs and mouse models of these diseases, including MPS-IIIA.[43] To assess the effect of the combina-

tion therapy on neuroinflammation compared to each monotherapy, frontal cortex and striatum were analyzed by immunohistochemistry (IHC) for astrogliosis and microgliosis using anti-glial fibrillary acidic protein (GFAP) and anti-ionized calcium binding adaptor molecule 1 (Iba1) antibodies, respectively. The analysis showed that the combination of gene therapy and CLR01 reduced the neuroinflammatory markers more efficiently than each single treatment (Figure 1A: GFAP cortex: $p < 0.0001$ MPS-IIIA combination therapy vs. MPS-IIIA CLR01; $p < 0.05$ MPS-IIIA combination therapy vs. MPS-IIIA AAV-*SGSH*. Striatum: $p < 0.0001$ MPS-IIIA combination therapy vs. MPS-IIIA CLR01; $p < 0.01$ MPS-IIIA combination therapy vs. MPS-IIIA AAV-*SGSH*. Figure S1: Iba1 cortex: $p < 0.05$ MPS-IIIA combination therapy vs. either MPS-IIIA CLR01 or MPS-IIIA AAV-*SGSH*. Striatum: $p < 0.01$ MPS-IIIA combined therapy vs. either MPS-IIIA CLR01 or MPS-IIIA AAV-*SGSH*. One-way ANOVA with Tukey's multiple comparison test). To corroborate these results, we quantified mRNA markers of activated astrocytes (H2T3 and Serping1) and microglia (interleukin-1 β [IL-1β] and tumor necrosis factor α [TNF-α]) in MPS-IIIA mouse brain using real-time PCR analysis. These markers were significantly reduced in MPS-IIIA mouse brain receiving either each monotherapy or the combination therapy. The p values for the differences among the three therapy groups were >0.05, yet the combination therapy consistently yielded the lowest mRNA level of each marker and the p values for the combination therapy compared to the mice receiving PBS (saline) for IL-1β, Serping1, and H23 (Figure 1B).

The combination therapy reduces lysosomal pathology and synaptic deficits in MPS-IIIA mice to a larger extent than each monotherapy

Lysosomal enlargement, a prominent pathological sign in MPS-IIIA mice, was assessed by IHC for LAMP1 and by electron microscopy (EM). As expected, MPS-IIIA mouse brains showed extensive enlargement of the lysosomal compartment compared to age-matched WT mice. This was evident both by a significantly increased signal in LAMP1 staining (Figure 2A) and the average lysosome size detected by EM (diameter >800 nm in MPS-IIIA mouse brains; Figure 2B). Although all the treatments reduced the lysosomal enlargement, the combined therapy decreased the LAMP1 signal and lysosomal size more efficiently than each monotherapy (Figure 2A: LAMP1 cortex: $p < 0.01$ for MPS-IIIA combined therapy vs. MPS-IIIA CLR01; $p < 0.05$ for MPS-IIIA combined therapy vs. MPS-IIIA AAV-*SGSH*. Striatum: $p < 0.01$ for MPS-IIIA combined therapy vs. MPS-IIIA CLR01; $p < 0.001$ for MPS-IIIA combined therapy vs. MPS-IIIA AAV-*SGSH*. Figure 2B: lysosomal size: $p < 0.01$ for MPS-IIIA combined therapy vs. MPS-IIIA CLR01; $p < 0.05$ MPS-IIIA combined therapy vs. MPS-IIIA AAV-*SGSH*. One-way ANOVA with Tukey's multiple comparison test).

Alterations of presynaptic structure and function are associated with lysosomal dysfunction in MPS-IIIA.[28] Consistently, reduced numbers of synaptic vesicles have been reported in mouse models of MPS, including MPS-IIIA.[7,28,44] EM analysis of cortical synapses showed that all treatments rescued the loss of synaptic vesicles, yet, again, the combined treatment rescued this loss significantly more efficiently than did the monotherapies (Figure 2C: synaptic vesicle/synaptic cleft length ratio: $p < 0.05$ for MPS-IIIA combined therapy vs. either MPS-IIIA CLR01 or MPS-IIIA AAV-*SGSH*. One-way ANOVA with Tukey's multiple comparison test).

Overall, these data demonstrate that CLR01 and AAV-mediated gene therapy act synergically and provide significantly improved therapeutic outcomes relative to each monotherapy. Therefore, the combination therapy can be considered superior to each treatment on its own.

The combination of CLR01 with gene therapy fully rescues behavioral deficits in MPS-IIIA mice

Our previous studies demonstrated that MPS-IIIA male mice develop a severe, age-dependent memory impairment in the contextual fear-conditioning test.[7,42] Here, we evaluated whether the combination therapy offered an advantage compared to the monotherapies. As expected, untreated 9-month-old MPS-IIIA mice showed a substantially reduced freezing time compared to WT mice (Figure 3A), indicating a memory deficit, and the monotherapies increased the freezing time compared to the untreated MPS-IIIA animals. However, a significant rescue of the memory deficit was observed in these experiments only in the combination therapy group (Figure 3A: percentage of freezing time: $p < 0.05$ for MPS-IIIA combined therapy vs. MPS-IIIA saline, two-way ANOVA with Tukey's multiple comparison test).

We also assessed the locomotor activity of the mice in the open field test. In agreement with previous findings,[45,46] measurements of distance traveled and immobility time showed a hypoactive behavior of MPS-IIIA mice compared to WT animals (Figure 3B). Neither gene therapy nor CLR01 alone significantly improved the distance traveled, yet, encouragingly, the combined therapy fully rescued this phenotype (Figure 3B). Immobility time was partially recovered by CLR01 but not by AAV-*SGSH* alone, whereas the combined therapy again fully rescued this behavioral deficit. The majority of the rescue may be attributed to the CLR01 treatment in this case because the improvement in the combination-therapy group was not significantly different from the CLR01 group. Nonetheless, the p values for the combination treatment were lower than those for the CLR01-only group compared to the saline control (Figure 3B: percentage of immobility time: $p < 0.001$ for MPS-IIIA combined therapy vs. MPS-IIIA saline and $p < 0.05$ for MPS-IIIA CLR01 vs. MPS-IIIA saline, one-way ANOVA with Tukey's multiple comparison test).

These data further demonstrate the advantage of the combination therapy compared to the AAV-mediated gene therapy or CLR01 treatment on their own in the MPS-IIIA mouse model.

The improved efficacy of the combined therapy is associated with enhanced clearance of amyloid deposits in MPS-IIIA mouse brain

We further addressed whether the mechanisms underlying the observed synergistic therapeutic effect were related to improved clearance of the toxic amyloid proteins in the MPS-IIIA mouse brain. GAG accumulation is thought to initiate and stabilize amyloid deposition, thus contributing to its storage in MPS.[35,47] Therefore, we evaluated whether the amyloid burden in the brain of the mice was relieved following mono- or combination therapies. The amyloid burden was analyzed using both thioflavin-S (ThS) staining, which measures total amyloid, and IHC staining of α-syn, the most abundant amyloidogenic protein found previously in the amyloid deposits.[7]

These analyses showed that although both the gene therapy and CLR01 on their own reduced the amyloid deposits significantly compared to MPS-IIIA mice treated with saline (Figure 4A: ThS staining: $p < 0.0001$ for either MPS-IIIA CLR01 or MPS-IIIA AAV-*SGSH* vs. MPS-IIIA saline. Figure 4B: IHC anti-α-syn: $p < 0.0001$ for either MPS-IIIA CLR01 or MPS-IIIA AAV-*SGSH* vs. MPS-IIIA saline. One-way ANOVA with Tukey's multiple comparison test.), substantial residual deposits remained compared to control WT mice (Figure 4A: ThS staining: $p < 0.05$ for MPS-IIIA CLR01 vs. WT saline; $p < 0.01$ for MPS-IIIA AAV-*SGSH* vs. WT saline. Figure 4B: IHC anti-α-syn: $p < 0.01$ for either MPS-IIIA CLR01 or MPS-IIIA AAV-*SGSH* vs. WT saline. One-way ANOVA with Tukey's multiple comparison test.). Notably, analysis of brain samples from a previous efficacy study. where AAV9-*SGSH* vectors were administered ICV at 5.4×10^{12} GCs/kg in 2-month-old MPS-IIIA mice,[42] highlighted the inability of this gene therapy to fully clear amyloid deposits in the MPS-IIIA mouse brain (Figure S2). Remarkably, however, the combination therapy reduced the amyloid deposit burden to
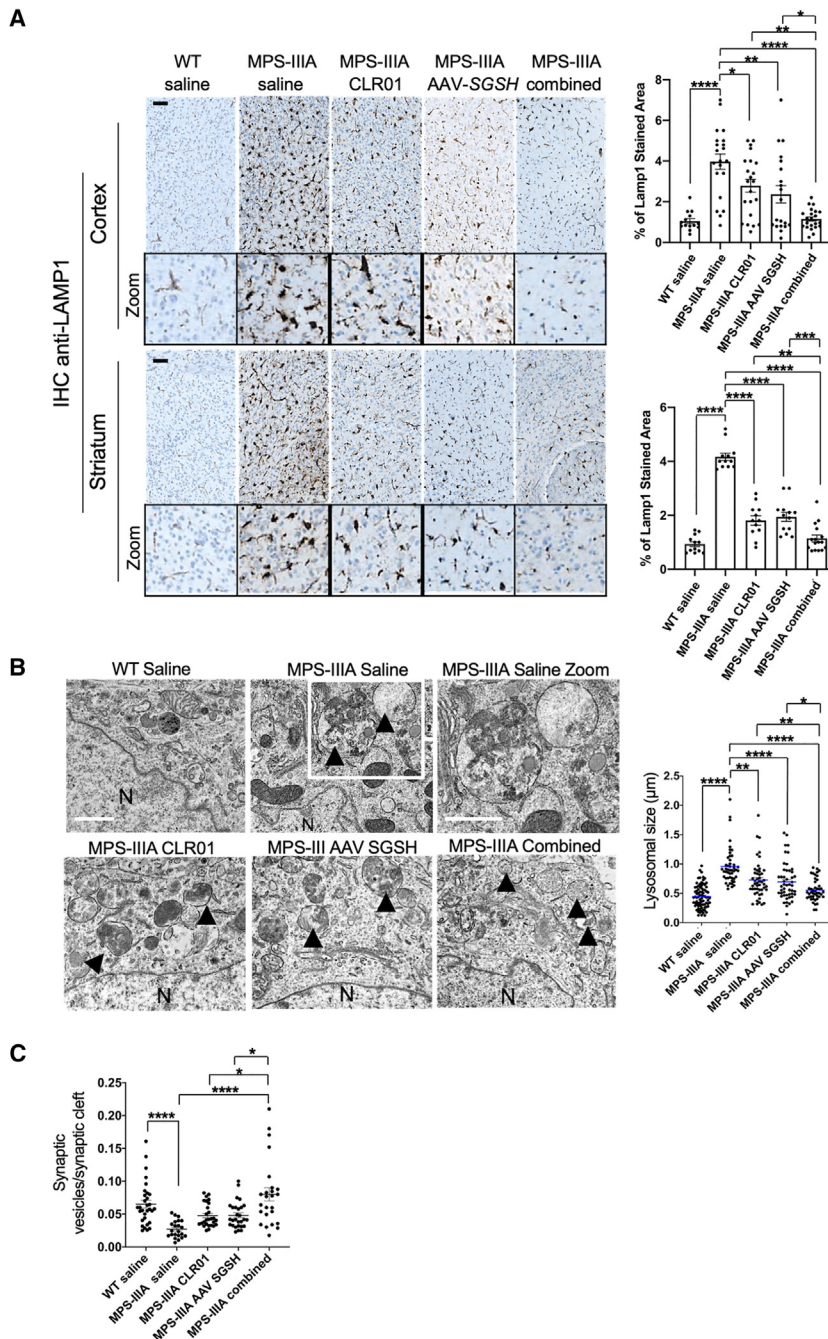
A

B

C

Figure 2. The combined therapy corrects lysosomal dysfunction and synaptic deficits more efficiently than the monotherapies

(A and B) MPS-IIIA and WT mice were analyzed for lysosomal enlargement by IHC using anti-LAMP1 antibodies (A) and EM analysis of lysosomal size (diameter of lysosomes) (B). Scale bars represent 30 μm (A) or 1 μm (B). Arrowheads indicate lysosomal-like structures; N = nuclei (B). The bar graphs in (A) show the percentage of LAMP1+ area quantified in 12–22 fields (represented by individual dots) from the cerebral frontal cortex or striatum of at least three mice for each experimental group. The data are presented as mean ± SEM. The size of lysosome-like structures was quantified for 45–49 lysosomes (represented by individual dots in the graph in B) from 15 cortical region fields of three animals for each experimental group. The data are presented as mean ± SEM. (C) Transmission electron microscopy analysis of synaptic-vesicle number was performed in the cerebral frontal cortex of MPS-IIIA and control mice. The bar graph shows the synaptic vesicles/synaptic cleft length ratio for 22–31 synapses (represented by individual dots) from three mice for each experimental group. The data are presented as mean ± SEM. *$p < 0.05$; **$p < 0.01$; ***$p < 0.001$; ****$p < 0.0001$. $p > 0.05$ are not presented. One-way ANOVA with Tukey's post hoc multiple comparison test.

burden, in agreement with the synergistic behavioral and pathological therapeutic effects. Notably, the SGSH activity levels in the brains of MPS-IIIA mice treated with AAV9-SGSH only were similar to those measured in MPS-IIIA mice treated with both CLR01 and AAV9-SGSH (Figure 4C). Consistently, the measurement of AAV vector copy number showed similar AAV transduction efficiency in the MPS-IIIA mouse brain treated with gene therapy and combined therapy (Figure 4D). Therefore, the observed synergistic effect observed upon addition of CLR01 treatment to AAV9-SGSH therapy was not due to an increased efficiency of the gene therapy, but rather most likely due to the reduction in the amyloid burden facilitated by CLR01.

The combination of AAV9-SGSH therapy and CLR01 is safe in MPS-IIIA mice

Although previously the AAV9-SGSH and CLR01 therapies have been shown to be safe in preclinical animal models,[41,48,49] to address whether together they might have caused unexpected safety concern, we evaluated the safety of the combination therapy. First, we assessed whether the treatment caused a significant change in body weight. The analysis showed that body weight did not change significantly in MPS-IIIA mice treated with the combination therapy compared to control WT mice or MPS-IIIA mice treated with saline (Figure S3A). We also assessed kidney weight as a marker of nephrotoxicity,[50] and the activity of aspartate transaminase (AST) and alanine

levels that were indistinguishable from those of the WT mice (Figure 4A: ThS staining: $p < 0.05$ MPS-IIIA combined therapy vs. MPS-IIIA CLR01 and $p < 0.01$ MPS-IIIA combined therapy vs. MPS-IIIA AAV-SGSH. One-way ANOVA with Tukey's multiple comparison test.). These results demonstrate that under our experimental settings, neither the gene therapy nor CLR01 alone fully cleared the secondary amyloid deposits in MPS-IIIA; however, the combined therapy successfully removed the persistent amyloid
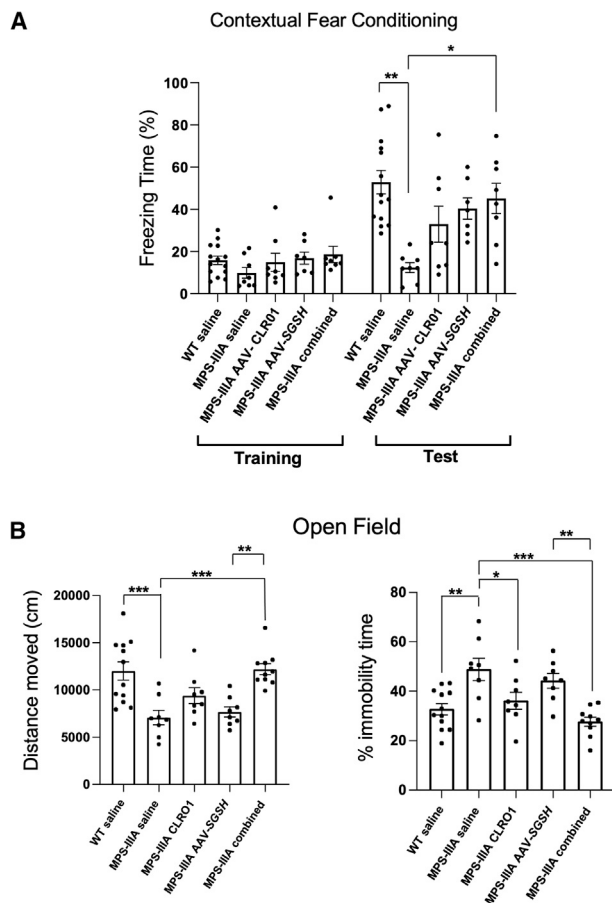
Figure 3. Behavioral correction in MPS-IIIA mice treated with combined therapy

(A and B) Memory function and exploratory activity were tested at 9 months of age in MPS-IIIA and control mice treated using the contextual fear-conditioning (A) and open field (B) tests. The percentage of time freezing during the fear-conditioning test, the total distance moved, and the percentage of immobility time in the open field test are presented as mean ± SEM. A total of 7–14 male mice (represented by individual dots) were tested in each group. *$p < 0.05$; **$p < 0.01$; ***$p < 0.001$; ****$p < 0.0001$. $p > 0.05$ are not presented. Open field test: one-way ANOVA with Tukey's post-hoc multiple comparison test. Fear-conditioning test: repeated measures two-way ANOVA followed by Tukey's post hoc test.

transaminase (ALT) in the blood as markers of liver damage. Kidney weight, AST activity, and ALT activity were increased significantly in MPS-IIIA mice treated with saline but were reduced to levels similar to those in WT animals (Figures S3B and S3C). This indicated not only that the combination therapy was safe but also that in addition to its neurotherapeutic effects, it corrected peripheral pathologic phenotypes in the MPS-IIIA mice.

Inhibiting amyloid deposition by CLR01 is effective in additional neuronopathic MPS mouse models

Given the therapeutic potential of CLR01 for the treatment of MPS-IIIA, we hypothesized that amyloid reduction mediated by CLR01

could also be beneficial in other neuronopathic MPSs. To test the hypothesis we used mouse models of MPS-I,[51] the most common form of MPS, and MPS-IIIC,[33] another severe neuronopathic form of Sanfilippo syndrome. These mouse models were generated by targeted disruption of the specific gene encoding the involved lysosomal enzyme (α-L-iduronidase [IDUA] and acetyl-coenzyme A:α-glucosaminide N-acetyltransferase [HGSNAT], respectively). Both mouse strains show a progressive CNS pathology, which recapitulates features observed in the human diseases and were shown to be useful for testing the preclinical efficacy of new therapeutic approaches.[33,44,51–54]

ThS staining of brain tissue from MPS-I and -IIIC mice at different ages showed that amyloid deposition was only minimal at 3 months of age but became robust at 5–6 months of age (Figure S4). Based on these findings, we initiated SC administration of 1 mg/kg CLR01 three times per week (the same as in the MPS-IIIA mice) at 3 months of age, before massive protein aggregation occurred (prevention paradigm). Mice were treated until 7 months of age, at which point they underwent behavioral testing and then were sacrificed for histopathological brain analysis. ThS staining revealed a significant and substantial reduction of amyloid deposition following CLR01 treatment in both MPS-I and -IIIC mice (Figures 5A and 5B). The decrease in amyloid deposition was associated with a significant reduction in both astrogliosis (GFAP staining) and lysosomal enlargement (LAMP1 staining) in the cortex (Figures 5A and 5B) and striatum (Figures S5A and S5B).

Memory function was evaluated using the fear-conditioning test. Similar to that in MPS-IIIA mice,[7,42] the test indicated a severe memory impairment in the MPS-I compared to WT mice, while it showed an "apparent" deficit in MPS-IIIC mice (freezing time was reduced in MPS-IIIC mice compared to WT control; however, the difference between the two groups was not statistically significant) (Figures 5C and 5D). CLR01 treatment significantly rescued the deficit in MPS-I mice (Figure 5C: percentage of freezing time: $p < 0.01$ for MPS-I CLR01 vs. MPS-I saline. Two-way ANOVA with Tukey's multiple comparison test.) and increased the freezing time in MPS-IIIC mice, although the difference between MPS-IIIC mice treated with CLR01 and control WT mice was not statistically significant (Figures 5C and 5D).

Overall, these results show that the strategy of reducing amyloid burden by treatment with CLR01 ameliorates the disease phenotype in two additional MPS mouse models, MPS-I and MPS-IIIC mice, extending the proof of efficacy beyond MPS-IIIA mice.

DISCUSSION

To date, no effective treatment exists to cure CNS pathology in MPS patients. Accumulation of amyloid deposits in neuronopathic MPS has been known for over 2 decades, yet it has only recently been recognized as a major contributor to the underlying pathologic processes. We have demonstrated that the accumulation of amyloid triggers lysosomal enlargement and reduces autophagosome fusion with lysosomes, thus impairing the autophagy flux, which in turn may exacerbate amyloid deposition in a vicious cycle.[7,35] Moreover, amyloids trigger inflammatory cascades in MPS by triggering microglia
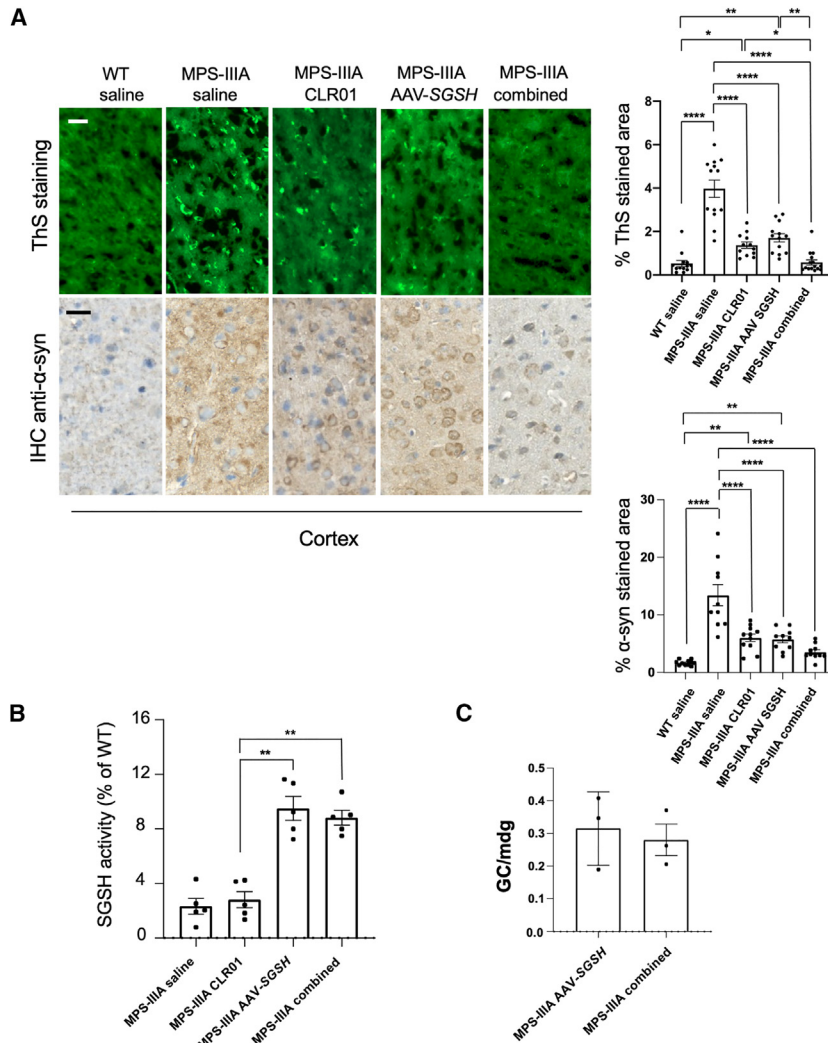
Figure 4. Amyloid protein deposits and AAV transduction in the brain of MPS-IIIA mice upon different treatments

(A) Amyloid deposition was analyzed in the frontal cortical regions of MPS-IIIA and control mice treated using ThS and α-syn staining. Persistent amyloid burden was observed following each monotherapy, whereas the combined treatment (AAV-*SGSH* + CLR01) reduced it to levels indistinguishable from those in WT mice. The bar graphs show the percentage of ThS fluorescence (top) quantified in 12–15 fields (represented by individual dots) and the percentage of α-syn⁺ staining (bottom) quantified in 10–11 fields (represented by individual dots) from the frontal cortical sections of three mice for each experimental group. Data are represented as mean ± SEM. Scale bars represent 30 μm in the ThS stain images and 15 μm in the α-syn-stained images. (B) Sulfamidase activity was measured in the MPS-IIIA mouse brain samples and expressed as a percentage of the activity found in age-matched WT mice treated with saline. Five animals (represented by individual dots) were used in each group. The data are presented as mean ± SEM. (C) The AAV vector copy number was measured in the MPS-IIIA mouse brain samples and expressed as GCs/mouse diploid genome (mdg). AAVs were undetectable in MPS-IIIA mouse brains treated with saline. Three animals (represented by individual dots) were used per group. Data are presented as mean ± SEM. $*p < 0.05$; $**p < 0.01$; $****p < 0.0001$. $p > 0.05$ are not presented. One-way ANOVA with Tukey's post hoc multiple comparison test.

we posit that anti-amyloid treatment should be considered as a therapeutic option more broadly in additional MPSs and LSDs.

Although our previous and current data have demonstrated clearly the benefit of the anti-amyloid strategy, this strategy on its own would be expected to have diminishing effects over time if applied to patients with MPS without addressing the primary enzymatic defect leading to lysosomal storage of GAGs. However, enzyme-corrective therapy strategies such as ERT and gene therapy have shown insufficient efficacy in clinical trials to date,[9–13] likely due to the inefficient inhibition of downstream neuropathologic cascades in the brains of patients with MPS. Therefore, we hypothesized that the combination of enzyme-corrective therapy with CLR01 would lead to improved outcomes compared to each monotherapy. Our current results clearly support this hypothesis.

Among therapies aimed at correcting the primary defect, we chose AAV-mediated gene therapy, a promising treatment approach for the neuronopathy in MPSs. We demonstrate that an AAV9-mediated gene delivery protocol correcting the primary storage of GAGs resulted in a synergistic therapeutic effect on several neurodegenerative phenotypes when applied to MPS-IIIA mice in combination with CLR01 to directly counteract the downstream amyloid accumulation.
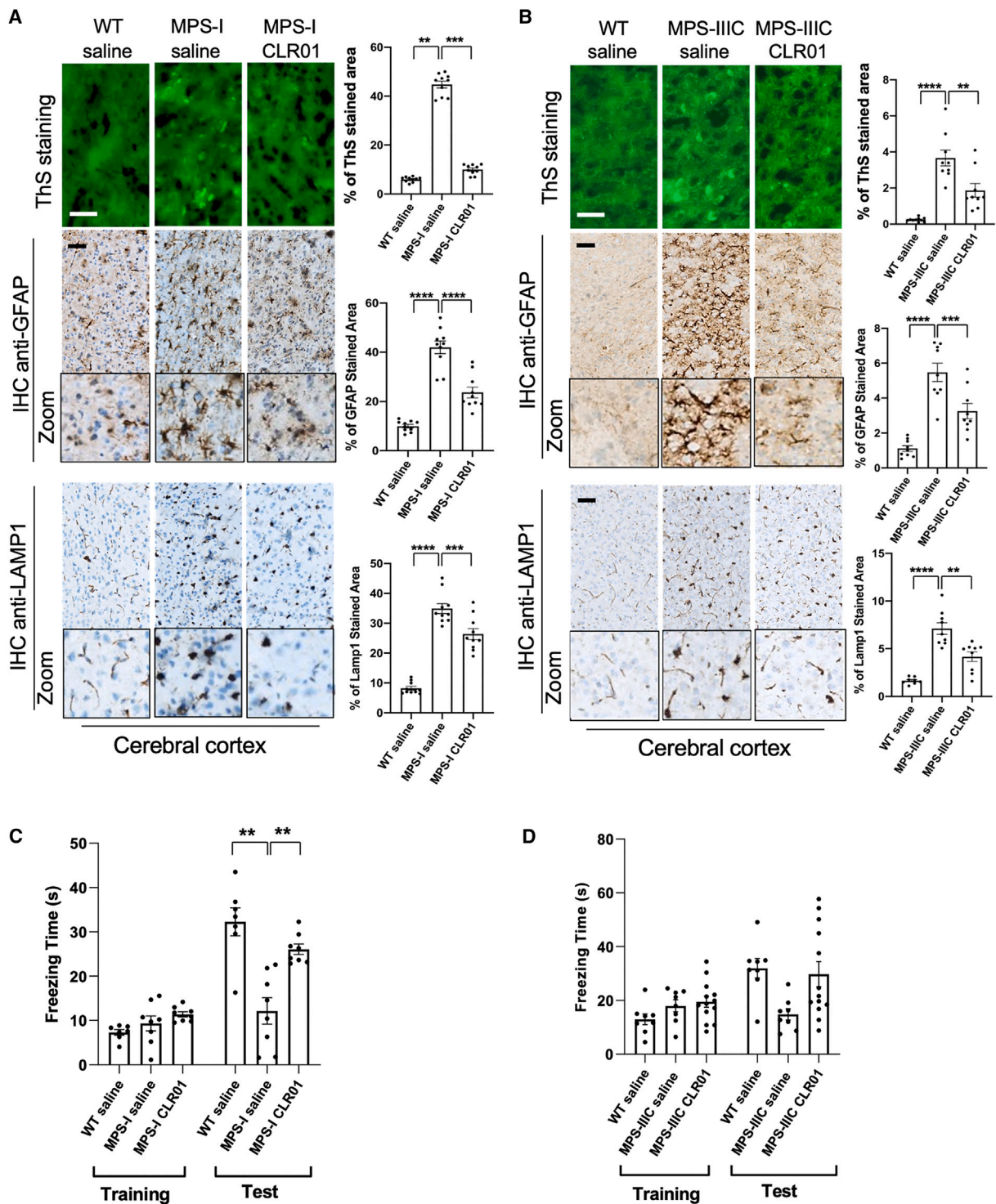
and astrocyte activation, leading to a destructive neuroinflammatory environment.[27,43] Of note, a recent clinical trial testing the anti-inflammatory IL-1R antagonist anakinra has shown significant improvement in multiple neurobehavioral domains of patients with MPS-III.[55] Therefore, amyloid storage is a key factor underlying multiple deleterious mechanisms downstream of the primary enzyme defect and GAG storage in different neuronopathic MPSs.

To date, targeting the secondary storage of toxic amyloidogenic proteins has only been explored for the treatment of neuronopathic MPS by our team. We demonstrated previously significant, beneficial, therapeutic effects of an anti-amyloid strategy in MPS-IIIA mice, in which daily SC injection of CLR01 between 4.5 and 9 months of age ameliorated lysosomal dysfunction and neuroinflammation and dramatically improved behavioral deficits in the mice in correlation with the reduced accumulation of amyloid aggregates.[7] Here, we showed that CLR01 achieved similar therapeutic effects in mouse models of two other neuronopathic MPSs, MPS-I and MPS-IIIC. Therefore,

Figure 5. CLR01 ameliorates multiple disease phenotypes in mouse models of MPS-I and MPS-IIIC

(A and B) MPS-I (A) and MPS-IIIC (B) mice were treated with 1.0 mg/kg CLR01 by SC injection three times per week starting at 3 months of age. WT mice on the same genetic background treated with saline were used as a control for both lines. At 7 months of age, we analyzed amyloid deposition (ThS staining), astrogliosis (GFAP staining), and lysosomal enlargement (LAMP1 staining) using sagittal brain sections. Enlarged images are shown for the IHC staining. Bar graphs to the right part of the images show the quantification of the ThS, GFAP, or LAMP1 staining in 8–10 different fields (represented by individual dots) from the cerebral frontal cortex of 3 mice per group. Data are

(legend continued on next page)

In agreement with previous studies, we show that targeting the enzyme defect and primary GAG storage by gene therapy reduces amyloid deposition in MPS-IIIA mice (Figures 3A and 3B), further supporting that GAG storage induces amyloid deposition.[35,47] However, gene therapy alone does not clear the secondary amyloid deposits in MPS-IIIA mice completely (Figures 3A, 3B, and S2). Rather, complete or near-complete reversal of the phenotype to the level of WT mice was achieved by combining the gene therapy with targeting the secondary storage directly by CLR01. Thanks to its concentration in lysosomes,[40] CLR01 both facilitates the degradation of existing amyloid stored in this compartment, which persists even when gene therapy is applied, and prevents the buildup of new amyloid. Importantly, the enhanced therapeutic effects cannot be explained by increased AAV transduction in the presence of CLR01 because both AAV copy number and sulfamidase activity in the brains of MPS-IIIA mice treated with the combination therapy were similar to those found in MPS-IIIA mice treated with AAV-*SGSH* only.

The preclinical data presented here suggest that the improved therapeutic effect achieved using the combined strategy may enhance the clinical efficacy in patients with MPS III (and potentially with other MPSs) by overcoming key challenges of the current gene-therapy protocols. For example, the combination of gene therapy with CLR01, maximizing the therapeutic effects, could employ the use of AAV vector doses lower than those used in currently exploited clinical trials based on AAV gene delivery alone, thus reducing toxic effect associated to high virus load.

Safety parameters evaluated in the MPS-IIIA mice treated with the combination therapy have shown not only a safe profile for the treatment but also protection from peripheral disease phenotypes, such as enlargement of kidneys and perturbation of liver enzymes (Figure S3). Formal safety studies evaluating potential side effects in WT mice and larger animals are planned in future studies to support clinical development of the combined therapy.

CLR01 is a broad-spectrum small molecule that has been shown to inhibit the aggregation and toxicity of ~20 amyloidogenic proteins and exert therapeutic effects on brain pathology upon systemic administration in multiple animal models of different neurodegenerative proteinopathies, including Alzheimer disease, Parkinson disease, and other tauopathies and synucleinopathies.[39,56–59] Moreover, CLR01 has a high safety profile and sufficient brain permeability for therapeutic applications.[48,59] Our preclinical efficacy studies in mouse models of neuronopathic MPSs confirm the safety, bioavailability, and neuroprotective effects of CLR01 administered systemically. Moreover, recent data show that CLR01 and other MTs concentrate in acidic cellular compartments, primarily in lysosomes and to a lesser extent in late endosomes and autophagosomes.[40] Elevated local concentrations in these compartments make MTs particularly efficacious for the treatment of lysosomal diseases, allowing them to achieve therapeutic effects at very low doses. Thus, neuronopathic MPSs represent ideal candidate diseases for testing the potential clinical translation of MTs.

In summary, we have demonstrated that targeting the secondary storage of amyloid by CLR01 is a broad-spectrum strategy that can be efficacious in multiple neuronopathic MPSs, and that coupling this strategy with gene therapy, and potentially other enzyme-corrective strategies, is a promising approach for enhancing the therapeutic potential and clinical translation of the treatment. Our findings support the further development of CLR01 and other MTs toward clinical translation for neuronopathic MPSs, with the prospect of making this approach the first line of therapy in the future when patients are screened for these diseases.

MATERIALS AND METHODS

Animals
MPS-IIIA mice (homozygous mutant for *Sgsh*),[34] MPS-I mice (homozygous *Idua*^{−/−}),[1] and MPS-IIIC mice (homozygous *Hgsnat*^{−/−}),[33] together with respective control littermate WT mice (*Sgsh*^{+/+}, *Idua*^{+/+}, and *Hgsna*^{+/+}), were utilized in this study. All mice were C57Bl/6 congenic. Animal studies were conducted in accordance with the guidelines of the Animal Care and Use Committee of CEINGE Advanced Biotechnologies Franco Salvatore in Naples and authorized by the Italian Ministry of Health (no. 495/2021-PR).

CLR01 administration
CLR01 was prepared in the Schrader lab, University of Duisburg-Essen, Germany. CLR01 powder was dissolved in PBS, pH 7.4, at 1.2 mg/mL. MPS-IIIA and WT mice were weighed, and a volume of the CLR01 solution corresponding to 1 mg/kg/day (50–60 μL solution per mouse) was injected SC three times per week. Control mice, both MPS-IIIA and WT, were injected similarly with PBS.

AVV production and administration
An expression cassette of human sulfamidase (*SGSH*) containing an alternative signal peptide of the iduronate 2-sulfatase (IDS) and a 3×FLAG tag attached to the C terminus[45] was cloned into a single-strand pAAV2.1-cytomegalovirus (CMV)-expression plasmid to generate the correspondent AAV serotype 9 viral vector according to protocols established at the InnovaVector AAV Vector Core. Mice 2.5 months old were anesthetized by intraperitoneal injection of ketamine (100 mg/kg) and xylazine (10 mg/kg) and placed on a stereotaxic instrument equipped with a motorized stereotaxic injector. A midline incision was made to expose the skull. A hole was drilled at bregma +0.5 mm anteroposterior, ±0.6 mm mediolateral, and −2.7 mm dorsoventral. A total of 4.5×10^{12} GCs/kg recombinant

---

presented as mean ± SEM. *p* values were calculated using one-way ANOVA with Tukey's post hoc multiple comparison test. (C and D) Memory function was measured at 7 months of age in MPS-I (C) and MPS-IIIC (D) mice along with control mice using the contextual fear-conditioning task. A total of 8–13 male mice (represented by individual dots) in each group were tested. Data are presented as mean ± SEM. *p* values were calculated using repeated-measures, two-way ANOVA with Tukey's post hoc test. **$p < 0.01$; ***$p < 0.001$; ****$p < 0.0001$. $p > 0.05$ are not presented.

AAV9 vectors encoding human IDS-SGSH-3×FLAG was injected into the lateral ventricles at a rate of 1 μL/min. After allowing the needle to remain in place for 5 min, the needle was slowly raised at a rate of 0.1 cm/min. Before each injection session in the animals used for the study, we carried out toluidine blue injections in control animals to test the effectiveness of the ICV injection procedure.

Tissue collection
Blood samples were collected by retro-orbital bleeding and then centrifuged at 3,000 rpm for 15 min to obtain serum. After euthanizing, mice from each experimental group were perfused with PBS to clear blood from the tissues, and kidney, liver, and brain were collected. The brains were divided into the two hemispheres: one was sectioned using a PA 002 Mouse Brain Blocker into five ~3-mm-thick sections (A, B, C, D, E) containing the main representative area of the CNS (A: olfactory bulb and prefrontal cortex; B: frontal cortex, lateral septum and basal ganglia regions; C: parietal cortex, hippocampus, striatum, thalamus; D: occipital cortex, pons, hippocampus; E: cerebellum, medulla oblongata, cervical region of spinal cord). Sections then were frozen in dry ice and used for biochemical analysis. The other hemisphere was fixed in 4% (w/v) paraformaldehyde (PFA) in PBS and embedded in paraffin or in optimal cutting temperature (OCT) compound upon sucrose incubation.

Brain cutting
Frozen OCT- or paraffin-embedded brain hemispheres were cut by the Advanced Histology Facility (AHF) at Telethon Institute of Genetics and Medicine (TIGEM). Specifically, the tissue was sectioned into 7-μm sagittal sections collected serially for each animal. Approximatively 30 serial sections were obtained from each hemisphere. For IHC, three serial sections at the same distance from the longitudinal fissure were analyzed. A schematic representation of tissue cutting is shown in Figure S6.

Brain homogenization
Brain sections were weighed and powdered in 6 vol Milli-Q water by using five freeze-thaw cycles and a mortar and pestle technique. Brain homogenates were either clarified (3,000 rpm for 10 min) and used for SGSH activity assay or used for RNA extraction.

SGSH activity assay
The brain homogenates were quantified for total protein content by a Bradford assay (emission 595 nm), and sulfamidase (SGSH) activity was measured as described previously[42] in the extracts of sections B, C, and D pooled together, representing the brain areas closest to the injection site.

AST and ALT assays in serum samples
Serum samples were collected from mice, and transaminase activities of AST and ALT were measured by Scil Vitro Vet analyzer.

Real-time PCR
Total RNA was isolated from MPS-IIIA and control brain homogenates using TriFastII (Euroclone) using a standard phenol/chloro-form extraction protocol. RNAs quality and concentration were evaluated spectrophotometrically using a NanoDrop instrument (A260/A280 was calculated to assess potential protein contamination). The potential contamination of genomic DNA was verified by electrophoresis. A total of 2 μg isolated RNA was reverse transcribed using the 5× All-In-One RT Master Mix (ABM) according to the manufacturer's instructions. Real-time PCR analyses were carried out on 100 ng cDNA, using BlasTaq 2X qPCR MasterMix kit (ABM) and SYBR Green as a detection system. Each primer was used at a final concentration of 250 nM. Experiments were performed using a 7900HT Fast Real-Time PCR System (Applied Biosystems) and the following protocol: an activation step of 2 min at 95°C followed by 40 cycles of denaturation for 5 s at 95°C, annealing for 30 s at 60°C, and extension for 30 s at 72°C. A single PCR product was present as confirmed by melt curve analysis. Gene expression was estimated using the comparative Ct (ΔCt, $\Delta\Delta$Ct) method, normalizing to the average of the endogenous housekeeping gene Actin.

The primer sequences were as follows:

TNF-α: forward 5′-ACTGAACTTCGGGGTGATCG-3′, reverse 5′-ACTGATGAGAGGGAGGCCAT-3′

IL-1β: forward 5′-TCGGACCCATATGAGCTGAAAG-3′, reverse 5′-CCACAGGTATTTTGTCGTTGCT-3′

H2T3: forward 5′-TCAGACCAGTATGCCCAACAG-3′, reverse 5′-AGCAGTGTTATCGTCTCCGTT-3′

Serping1: forward 5′-GAACTTGGACCAGGACGCA-3′, reverse 5′-TCGGGATCTGAGAAGGCTCT-3′

Actin: forward 5′-GGCTGTATTCCCCTCCATCG -3′, reverse 5′-CCAGTTGGTAACAATGCCATGT-3′

AAV vector copy-number analysis
Genomic DNA was isolated from brain homogenates using TriFast II (Euroclone), and its concentration was estimated using a NanoDrop instrument. Real-time PCR was carried on 100 ng of extracted DNA using BlasTaq 2X qPCR MasterMix as a detection kit. Experiments were performed using a 7900HT Fast Real-Time PCR System (Applied Biosystems) and the following protocol: 2 min at 50°C, 10 min at 95°C, followed by 40 cycles of 15 s at 95°C and 1 min at 60°C. Forward (5′-CCGCCATGCTACTTATCTACGTAGC-3′) and reverse (5′-CGGTAGACAACAAACGGGGAGG-3′) primers were used at final a concentration of 250 nM. Genome copies were measured using a standard curve created using plasmid pAAV2.1-CMV-IDSspSGSH.

Antibodies
The following antibodies and dilutions were used: polyclonal rabbit anti-α-synuclein (128102, Synaptic System, IHC: 1:300), polyclonal rabbit anti-GFAP (Z0334, DAKO Agilent, IHC: 1:400), polyclonal rabbit anti-IBA 1 (019–19741, Wako, IHC: 1:200), polyclonal rabbit anti-LC3 (PM036, MBL, immunofluorescence [IF]: 1:1,000), monoclonal rat anti-Lamp1 (SC-19992, Santa Cruz, IF: 1:300), polyclonal

rabbit anti-Lamp1 (ab24170, Abcam, IHC: 1:200), monoclonal mouse anti-β-Actin (E-AB-20031, Elabscience Biotechnology), goat anti-mouse immunoglobulin G(H + L) (peroxidase/horseradish peroxidase [HRP] conjugated, E-AB-1001, Elabscience Biotechnology). Alexa Fluor secondary antibodies used in IF experiments were purchased from Molecular Probe (Invitrogen).

Proteinase K treatment

Proteinase K digestion was performed for α-syn IHC protocol as described previously.[7] Briefly, after rehydration, 7-μm-thick paraffin-embedded sections were treated with 3% H_2O_2 for 1 h to quench the endogenous peroxidases. Proteinase K (Euroclone) was added at a concentration of 50 μg/mL for 2 min at 37°C. Unmasking was performed by incubating the sections for 10 min in a citrate buffer, pH 6, in a microwave oven. After blocking by using 5% (w/v) BSA in PBS, sections were incubated with the specific antibodies.

IHC

Automated IHC

IHC standardized assays were performed by the AHF at TIGEM on brain tissue sections using a VENTANA BenchMark Ultra automated staining instrument (Ventana Medical Systems, Roche) and VENTANA reagents except as noted, according to the manufacturer's instructions. Paraffin-embedded sections were deparaffinized using wash buffer (catalog no. 950–510) for 16 min at 72°C. Epitope retrieval was accomplished using CC1 solution (catalog no. 950–500) at 95°C for 10 min. Antibodies were diluted using a blocking solution into user-fillable dispensers for use on the automated stainer. For bright-field detection, slides were developed using the Discovery ChromoMap DAB kit (catalog no. 760-159) according to the manufacturer's instructions. Slides were then counterstained with hematoxylin II (catalog no. 790–2208) for 8 min, followed by bluing reagent (catalog no. 760–2037) for 4 min. Bright-field sections were scanned using a ZEISS Axio Scan.Z1 microscope. Whole digital slides were viewed by ZEN Blue software.

Non-automated IHC (α-syn IHC)

Paraffin-embedded sections were deparaffinized with xylene and then incubated in ethanol scale to re-hydrate sections. Staining was performed using the Vectastain Elite ABC-HRP Kit (PK6200, Vector Laboratories). Visualization was performed using 3,3-diaminobenzidine (DAB) tetrahydrochloride (Vector Laboratories). Stained slides were scanned using a Hamamatsu Nanozoomer 2.0-RS scanner and viewed with NDP.view2.

IHC quantitation

Quantitation of the immunostained area was performed by using the tool "measure" in ImageJ after the conversion of the images to an 8-bit format and adjusting the threshold to a fixed value.

ThS staining

OCT-embedded sections, 7 μm, were incubated in 0.01% (w/v) ThS (T1892, Sigma) dissolved in ethanol for 10 min. Slides were washed in PBS 3 times and mounted using Vectashield mounting medium. Positive staining and scan of the entire section were obtained using a Zeiss Apotome.2 Imager.M2 using the GFP filter.

EM

EM was performed using the tools and protocols of TIGEM Advanced Microscopy and Image facility. Cortex regions (slice C) were fixed in 1% glutaraldehyde and 4% PFA in 200 mM HEPES, pH 7.3, for 10 min at 37°C, post-fixed in 1% osmium tetroxide, dehydrated, and embedded in resin. Ultrathin sections were cut using a LEICA EM UC7 ultramicrotome. Lysosome size and number were evaluated using the software iTEM (Olympus). "Lysosomes" were identified by morphometric analysis as a wide spectrum of lysosome-like structures that includes bona fide lysosomes, autolysosomes, multi-vesicular bodies, and vacuoles containing stored undigested material.

Behavioral analysis

Behavioral tests were carried out in a behavioral testing room maintained under constant light, temperature, and humidity. The mice were tested during daylight hours (between 9 a.m. and 6 p.m.). Before testing, animals were habituated to the testing room for at least 30 min. We used only male MPS-IIIA mice, as differences in disease progression have been reported previously between female and male mice.[42,46,60]

Contextual fear-conditioning test

The contextual fear-conditioning task allows the evaluation of the ability of the mouse to learn and remember a Pavlovian association between a mild electrical foot shock and a specific context. Each mouse was trained in a conditioning chamber (30 × 24 × 21 cm; Ugo Basile) equipped with a removable grid floor and waste pan. The grid floor contained 36 stainless-steel rods (3 mm diameter) spaced 8 mm center to center. When placed in the chamber, the grid floor contacted a circuit board through which scrambled shock was delivered. The shock intensity was 0.5 mA with a duration of 2 s, and it was presented three times and associated with a context. At 24 h after training, the mice were tested using the same context but in the absence of the foot shock. Freezing behavior was defined as a complete lack of movement, except for respiration, and scored using a video tracking system (ANY-MAZE, Stoelting).

Open field test

The open field test allows evaluating the emotional changes and locomotor ability of the mouse. It was carried out in a chamber measuring 40 cm in length, 40 cm in width, and 30 cm in height, made of white, high-density, non-porous plastic. The chamber was divided into periphery (40 × 40 cm), transition zone (30 × 30 cm), and center (10 × 10 cm), designated in Nordus Ethovision XT 17 software. Each mouse was placed in the chamber and was allowed to freely explore the field for 30 min. The course was recorded using a Basler Emulation video camera (0815-0000), and the immobility time, the time in the center zone, and distance traveled were extracted from the video recordings.

Statistical analysis

All the data are expressed as mean ± SEM. Data in the open field test and comparisons of brain pathology were analyzed using a one-way ANOVA with Tukey's post hoc multiple comparison test. The fear-conditioning test was analyzed using a two-way ANOVA for repeated measures with the factor group as an independent factor and trials or test phase as repeated measures to assess differences among multiple experimental groups at different time points, followed by Tukey's post hoc test when appropriate. A $p < 0.05$ was considered statistically significant.

DATA AND CODE AVAILABILITY

The authors declare that the data supporting the findings of this study are available within the main text and the supplemental figures.

AUTHOR CONTRIBUTIONS

M.G. and A.M performed research and analyzed the data. L.G. performed and analyzed most of the behavioral studies. A.P and L.B contributed to the IHC data. R.R. contributed to behavioral studies. F.-G.K., D.K., and T.S. performed the CLR01 production. C.P. and P.P. performed the AST and ALT experiments; M.M. helped with the IHC interpretation and manuscript proofreading. X.P. and A.V.P. provided the MPS-IIIC mice and performed ThS in MPS-IIIC brains. M.K., I.S., and G.B. contributed to data interpretation and manuscript writing. N.C.S. contributed to the interpretation and analysis of the IHC data. A.F. designed and supervised the research and wrote the manuscript.

DECLARATION OF INTERESTS

The compositions of matter (patent 1, application 2) and methods of use (applications 3 and 4) of CLR01 are protected by the patents and patent applications listed below. G.B. and T.S. are co-inventors on 1 and 2. A.F. and G.B. are co-inventors on 3 and 4.

1. International Patent no. PCT/US2010/026419, USA patent no. 8,791,092, European patent no. EP2403859 A2
2. International Patent Application no. PCT/US2019/039943, US Patent Application no. 17/255,963, EU Application no. 19824 953.4
3. International Patent Application no. PCT/US2019/029221, EU Application no. 19850534.9
4. International Patent Application no. PCT/US2019/029222, EU Application no. 19841367.6

SUPPLEMENTAL INFORMATION

Supplemental information can be found online at https://doi.org/10.1016/j.ymthe.2024.09.030.

REFERENCES

1. Clarke, L.A. (2008). The mucopolysaccharidoses: a success of molecular medicine. Expert Rev. Mol. Med. 10, e1. https://doi.org/10.1017/S1462399408000550.

2. Neufeld, E.F., Muenzer, J., Scriver, C., Beaudet, A.L., Sly, W.S., and Valle, D. (2001). In The Metabolic and Molecular Bases of Inherited Disease, C. Scriver, A.L. Beaudet, D. Valle, and W. Sly, eds.

3. Ballabio, A. (2009). Disease pathogenesis explained by basic science: lysosomal storage diseases as autophagocytic disorders. Int. J. Clin. Pharmacol. Ther. 47, S34–S38. https://doi.org/10.5414/cpp47034.

4. Lieberman, A.P., Puertollano, R., Raben, N., Slaugenhaupt, S., Walkley, S.U., and Ballabio, A. (2012). Autophagy in lysosomal storage disorders. Autophagy 8, 719–730. https://doi.org/10.4161/auto.19469.

5. Settembre, C., Fraldi, A., Rubinsztein, D.C., and Ballabio, A. (2008). Lysosomal storage diseases as disorders of autophagy. Autophagy 4, 113–114. https://doi.org/10.4161/auto.5227.

6. Pierzynowska, K., Gaffke, L., Podlacha, M., Brokowska, J., and Węgrzyn, G. (2020). Mucopolysaccharidosis and Autophagy: Controversies on the[1] Contribution of the Process to the Pathogenesis and Possible Therapeutic Applications. Neuromolecular Med. 22, 25–30. https://doi.org/10.1007/s12017-019-08559-1.

7. Monaco, A., Maffia, V., Sorrentino, N.C., Sambri, I., Ezhova, Y., Giuliano, T., Cacace, V., Nusco, E., De Risi, M., De Leonibus, E., et al. (2020). The Amyloid Inhibitor CLR01 Relieves Autophagy and Ameliorates Neuropathology in a Severe Lysosomal Storage Disease. Mol. Ther. 28, 1167–1176. https://doi.org/10.1016/j.ymthe.2020.02.005.

8. Fraldi, A., Serafini, M., Sorrentino, N.C., Gentner, B., Aiuti, A., and Bernardo, M.E. (2018). Gene therapy for mucopolysaccharidoses: in vivo and ex vivo approaches. Ital. J. Pediatr. 44, 130. https://doi.org/10.1186/s13052-018-0565-y.

9. Taylor, M., Khan, S., Stapleton, M., Wang, J., Chen, J., Wynn, R., Yabe, H., Chinen, Y., Boelens, J.J., Mason, R.W., et al. (2019). Hematopoietic Stem Cell Transplantation for Mucopolysaccharidoses: Past, Present, and Future. Biol. Blood Marrow Transpl. 25, e226–e246. https://doi.org/10.1016/j.bbmt.2019.02.012.

10. Christensen, C.L., Ashmead, R.E., and Choy, F.Y.M. (2019). Cell and Gene Therapies for Mucopolysaccharidoses: Base Editing and Therapeutic Delivery to the CNS. Diseases 7, 47. https://doi.org/10.3390/diseases7030047.

11. Sato, Y., and Okuyama, T. (2020). Novel Enzyme Replacement Therapies for Neuropathic Mucopolysaccharidoses. Int. J. Mol. Sci. 21, 400. https://doi.org/10.3390/ijms21020400.

12. de Castro, M.J., Del Toro, M., Giugliani, R., and Couce, M.L. (2021). Gene Therapy for Neuronopathic Mucopolysaccharidoses: State of the Art. Int. J. Mol. Sci. 22, 9200. https://doi.org/10.3390/ijms22179200.

13. Wood, S.R., and Bigger, B.W. (2022). Delivering gene therapy for mucopolysaccharide diseases. Front. Mol. Biosci. 9, 965089. https://doi.org/10.3389/fmolb.2022.965089.

14. Marcò, S., Haurigot, V., and Bosch, F. (2019). In Vivo Gene Therapy for Mucopolysaccharidosis Type III (Sanfilippo Syndrome): A New Treatment Horizon. Hum. Gene Ther. 30, 1211–1221. https://doi.org/10.1089/hum.2019.217.

15. Cantore, A., Fraldi, A., Meneghini, V., and Gritti, A. (2021). In vivo Gene Therapy to the Liver and Nervous System: Promises and Challenges. Front. Med. 8, 774618. https://doi.org/10.3389/fmed.2021.774618.

16. Tardieu, M., Zérah, M., Husson, B., de Bournonville, S., Deiva, K., Adamsbaum, C., Vincent, F., Hocquemiller, M., Broissand, C., Furlan, V., et al. (2014). Intracerebral administration of adeno-associated viral vector serotype rh.10 carrying human SGSH and SUMF1 cDNAs in children with mucopolysaccharidosis type IIIA disease: results of a phase I/II trial. Hum. Gene Ther. 25, 506–516. https://doi.org/10.1089/hum.2013.238.

17. Tardieu, M., Zérah, M., Gougeon, M.L., Ausseil, J., de Bournonville, S., Husson, B., Zafeiriou, D., Parenti, G., Bourget, P., Poirier, B., et al. (2017). Intracerebral gene therapy in children with mucopolysaccharidosis type IIIB syndrome: an uncontrolled phase 1/2 clinical trial. Lancet Neurol. 16, 712–720. https://doi.org/10.1016/S1474-4422(17)30169-2.

18. Seker Yilmaz, B., Davison, J., Jones, S.A., and Baruteau, J. (2021). Novel therapies for mucopolysaccharidosis type III. J. Inherit. Metab. Dis. 44, 129–147. https://doi.org/10.1002/jimd.12316.

19. Hinderer, C., Katz, N., Buza, E.L., Dyer, C., Goode, T., Bell, P., Richman, L.K., and Wilson, J.M. (2018). Severe Toxicity in Nonhuman Primates and Piglets Following High-Dose Intravenous Administration of an Adeno-Associated Virus Vector Expressing Human SMN. Hum. Gene Ther. 29, 285–298. https://doi.org/10.1089/hum.2018.015.

20. Garbuzova-Davis, S., Mirtyl, S., Sallot, S.A., Hernandez-Ontiveros, D.G., Haller, E., and Sanberg, P.R. (2013). Blood-brain barrier impairment in MPS III patients. BMC Neurol. 13, 174. https://doi.org/10.1186/1471-2377-13-174.

21. Harmatz, P., Lau, H.A., Heldermon, C., Leslie, N., Foo, C.W.P., Vaidya, S.A., and Whitley, C.B. (2019/02/01/2019). EMPOWERS: A phase 1/2 clinical trial of SB-318 ZFN-mediated in vivo human genome editing for treatment of MPS I (Hurler syndrome). Mol. Genet. Metab. 126, S68. https://doi.org/10.1016/j.ymgme.2018.12.163.

22. Ginsberg, S.D., Galvin, J.E., Lee, V.M., Rorke, L.B., Dickson, D.W., Wolfe, J.H., Jones, M.Z., and Trojanowski, J.Q. (1999). Accumulation of intracellular amyloid-β peptide (A β 1-40) in mucopolysaccharidosis brains. J. Neuropathol. Exp. Neurol. 58, 815–824. https://doi.org/10.1097/00005072-199908000-00004.

23. Hamano, K., Hayashi, M., Shioda, K., Fukatsu, R., and Mizutani, S. (2008). Mechanisms of neurodegeneration in mucopolysaccharidoses II and IIIB: analysis of human brain tissue. Acta Neuropathol. 115, 547–559. https://doi.org/10.1007/s00401-007-0325-3.

24. Viana, G.M., Priestman, D.A., Platt, F.M., Khan, S., Tomatsu, S., and Pshezhetsky, A.V. (2020). Brain Pathology in Mucopolysaccharidoses (MPS) Patients with Neurological Forms. J. Clin. Med. 9, 396. https://doi.org/10.3390/jcm9020396.

25. Viana, G.M., Gonzalez, E.A., Alvarez, M.M.P., Cavalheiro, R.P., do Nascimento, C.C., Baldo, G., D'Almeida, V., de Lima, M.A., Pshezhetsky, A.V., and Nader, H.B. (2020). Cathepsin B-associated Activation of Amyloidogenic Pathway in Murine Mucopolysaccharidosis Type I Brain Cortex. Int. J. Mol. Sci. 21, 1459. https://doi.org/10.3390/ijms21041459.

26. Beard, H., Hassiotis, S., Gai, W.P., Parkinson-Lawrence, E., Hopwood, J.J., and Hemsley, K.M. (2017). Axonal dystrophy in the brain of mice with Sanfilippo syndrome. Exp. Neurol. 295, 243–255. https://doi.org/10.1016/j.expneurol.2017.06.010.

27. Parker, H., Ellison, S.M., Holley, R.J., O'Leary, C., Liao, A., Asadi, J., Glover, E., Ghosh, A., Jones, S., Wilkinson, F.L., et al. (2020). Haematopoietic stem cell gene therapy with IL-1Ra rescues cognitive loss in mucopolysaccharidosis IIIA. EMBO Mol. Med. 12, e11185. https://doi.org/10.15252/emmm.201911185.

28. Sambri, I., D'Alessio, R., Ezhova, Y., Giuliano, T., Sorrentino, N.C., Cacace, V., De Risi, M., Cataldi, M., Annunziato, L., De Leonibus, E., and Fraldi, A. (2017). Lysosomal dysfunction disrupts presynaptic maintenance and restoration of presynaptic function prevents neurodegeneration in lysosomal storage diseases. EMBO Mol. Med. 9, 112–132. https://doi.org/10.15252/emmm.201606965.

29. Capuozzo, A., Montefusco, S., Cacace, V., Sofia, M., Esposito, A., Napolitano, G., Nusco, E., Polishchuk, E., Pizzo, M.T., De Risi, M., et al. (2022). Fluoxetine ameliorates mucopolysaccharidosis type IIIA. Mol. Ther. 30, 1432–1450. https://doi.org/10.1016/j.ymthe.2022.01.037.

30. Ohmi, K., Zhao, H.Z., and Neufeld, E.F. (2011). Defects in the medial entorhinal cortex and dentate gyrus in the mouse model of Sanfilippo syndrome type B. PLoS One 6, e27461. https://doi.org/10.1371/journal.pone.0027461.

31. Kan, S.H., Aoyagi-Scharber, M., Le, S.Q., Vincelette, J., Ohmi, K., Bullens, S., Wendt, D.J., Christianson, T.M., Tiger, P.M.N., Brown, J.R., et al. (2014). Delivery of an enzyme-IGFII fusion protein to the mouse brain is therapeutic for mucopolysaccharidosis type IIIB. Proc. Natl. Acad. Sci. USA 111, 14870–14875. https://doi.org/10.1073/pnas.1416660111.

32. Naughton, B.J., Duncan, F.J., Murrey, D., Ware, T., Meadows, A., McCarty, D.M., and Fu, H. (2013). Amyloidosis, synucleinopathy, and prion encephalopathy in a neuropathic lysosomal storage disease: the CNS-biomarker potential of peripheral blood. PLoS One 8, e80142. https://doi.org/10.1371/journal.pone.0080142.

33. Martins, C., Hůlková, H., Dridi, L., Dormoy-Raclet, V., Grigoryeva, L., Choi, Y., Langford-Smith, A., Wilkinson, F.L., Ohmi, K., DiCristo, G., et al. (2015). Neuroinflammation, mitochondrial defects and neurodegeneration in mucopolysaccharidosis III type C mouse model. Brain 138, 336–355. https://doi.org/10.1093/brain/awu355.

34. Bhaumik, M., Muller, V.J., Rozaklis, T., Johnson, L., Dobrenis, K., Bhattacharyya, R., Wurzelmann, S., Finamore, P., Hopwood, J.J., Walkley, S.U., and Stanley, P. (1999). A mouse model for mucopolysaccharidosis type III A (Sanfilippo syndrome). Glycobiology 9, 1389–1396. https://doi.org/10.1093/glycob/9.12.1389.

35. Monaco, A., and Fraldi, A. (2020). Protein Aggregation and Dysfunction of Autophagy-Lysosomal Pathway: A Vicious Cycle in Lysosomal Storage Diseases. Front. Mol. Neurosci. 13, 37. https://doi.org/10.3389/fnmol.2020.00037.

36. Attar, A., and Bitan, G. (2014). Disrupting self-assembly and toxicity of amyloidogenic protein oligomers by "molecular tweezers" - from the test tube to animal models. Curr. Pharm. Des. 20, 2469–2483. https://doi.org/10.2174/13816128113199990496.

37. Schrader, T., Bitan, G., and Klärner, F.G. (2016). Molecular tweezers for lysine and arginine - powerful inhibitors of pathologic protein aggregation. Chem. Commun. 52, 11318–11334. https://doi.org/10.1039/c6cc04640a.

38. Hadrovic, I., Rebmann, P., Klärner, F.G., Bitan, G., and Schrader, T. (2019). Molecular Lysine Tweezers Counteract Aberrant Protein Aggregation. Front. Chem. 7, 657. https://doi.org/10.3389/fchem.2019.00657.

39. Shahpasand-Kroner, H., Siddique, I., Malik, R., Linares, G.R., Ivanova, M.I., Ichida, J., Weil, T., Münch, J., Sanchez-Garcia, E., Klärner, F.G., et al. (2023). Molecular Tweezers: Supramolecular Hosts with Broad-Spectrum Biological Applications. Pharmacol. Rev. 75, 263–308. https://doi.org/10.1124/pharmrev.122.000654.

40. Li, Z., Siddique, I., Hadrović, I., Kirupakaran, A., Li, J., Zhang, Y., Klärner, F.G., Schrader, T., and Bitan, G. (2021). Lysine-selective molecular tweezers are cell penetrant and concentrate in lysosomes. Commun. Biol. 4, 1076. https://doi.org/10.1038/s42003-021-02603-2.

41. Haurigot, V., Marcó, S., Ribera, A., Garcia, M., Ruzo, A., Villacampa, P., Ayuso, E., Añor, S., Andaluz, A., Pineda, M., et al. (2013). Whole body correction of mucopolysaccharidosis IIIA by intracerebrospinal fluid gene therapy. J. Clin. Invest. 123, 3254–3271. https://doi.org/10.1172/JCI66778.

42. Sorrentino, N.C., Cacace, V., De Risi, M., Maffia, V., Strollo, S., Tedesco, N., Nusco, E., Romagnoli, N., Ventrella, D., Huang, Y., et al. (2019). Enhancing the Therapeutic Potential of Sulfamidase for the Treatment of Mucopolysaccharidosis IIIA. Mol. Ther. Methods Clin. Dev. 15, 333–342. https://doi.org/10.1016/j.omtm.2019.10.009.

43. Parker, H., and Bigger, B.W. (2019). The role of innate immunity in mucopolysaccharide diseases. J. Neurochem. 148, 639–651. https://doi.org/10.1111/jnc.14632.

44. Wilkinson, F.L., Holley, R.J., Langford-Smith, K.J., Badrinath, S., Liao, A., Langford-Smith, A., Cooper, J.D., Jones, S.A., Wraith, J.E., Wynn, R.F., et al. (2012). Neuropathology in mouse models of mucopolysaccharidosis type I, IIIA and IIIB. PLoS One 7, e35787. https://doi.org/10.1371/journal.pone.0035787.

45. Sorrentino, N.C., D'Orsi, L., Sambri, I., Nusco, E., Monaco, C., Spampanato, C., Polishchuk, E., Saccone, P., De Leonibus, E., Ballabio, A., and Fraldi, A. (2013). A highly secreted sulphamidase engineered to cross the blood-brain barrier corrects brain lesions of mice with mucopolysaccharidoses type IIIA. EMBO Mol. Med. 5, 675–690. https://doi.org/10.1002/emmm.201202083.

46. De Risi, M., Tufano, M., Alvino, F.G., Ferraro, M.G., Torromino, G., Gigante, Y., Monfregola, J., Marrocco, E., Pulcrano, S., Tunisi, L., et al. (2021). Altered heparan sulfate metabolism during development triggers dopamine-dependent autistic-behaviours in models of lysosomal storage disorders. Nat. Commun. 12, 3495. https://doi.org/10.1038/s41467-021-23903-5.

47. Iannuzzi, C., Irace, G., and Sirangelo, I. (2015). The effect of glycosaminoglycans (GAGs) on amyloid aggregation and toxicity. Molecules 20, 2510–2528. https://doi.org/10.3390/molecules20022510.

48. Attar, A., Chan, W.T.C., Klärner, F.G., Schrader, T., and Bitan, G. (2014). Safety and pharmacological characterization of the molecular tweezer CLR01 – a broad-spectrum inhibitor of amyloid proteins' toxicity. BMC Pharmacol. Toxicol. 15, 23. https://doi.org/10.1186/2050-6511-15-23.

49. Sorrentino, N.C., Maffia, V., Strollo, S., Cacace, V., Romagnoli, N., Manfredi, A., Ventrella, D., Dondi, F., Barone, F., Giunti, M., et al. (2016). A Comprehensive Map of CNS Transduction by Eight Recombinant Adeno-associated Virus Serotypes Upon Cerebrospinal Fluid Administration in Pigs. Mol. Ther. 24, 276–286. https://doi.org/10.1038/mt.2015.212.

50. Antognini, N., Portman, R., Dong, V., Webb, N.J., and Chand, D.H. (2024). Detection, Monitoring, and Mitigation of Drug-Induced Nephrotoxicity: A Pragmatic Approach. Ther. Innov. Regul. Sci. 58, 286–302. https://doi.org/10.1007/s43441-023-00599-x.

51. Clarke, L.A., Russell, C.S., Pownall, S., Warrington, C.L., Borowski, A., Dimmick, J.E., Toone, J., and Jirik, F.R. (1997). Murine mucopolysaccharidosis type I: targeted disruption of the murine alpha-L-iduronidase gene. Hum. Mol. Genet. 6, 503–511.

52. Ohmi, K., Greenberg, D.S., Rajavel, K.S., Ryazantsev, S., Li, H.H., and Neufeld, E.F. (2003). Activated microglia in cortex of mouse models of mucopolysaccharidoses I

and IIIB. Proc. Natl. Acad. Sci. USA *100*, 1902–1907. https://doi.org/10.1073/pnas.252784899.

53. Li, H.H., Yu, W.H., Rozengurt, N., Zhao, H.Z., Lyons, K.M., Anagnostaras, S., Fanselow, M.S., Suzuki, K., Vanier, M.T., and Neufeld, E.F. (1999). Mouse model of Sanfilippo syndrome type B produced by targeted disruption of the gene encoding alpha-N-acetylglucosaminidase. Proc. Natl. Acad. Sci. USA *96*, 14505–14510. https://doi.org/10.1073/pnas.96.25.14505.

54. Heldermon, C.D., Hennig, A.K., Ohlemiller, K.K., Ogilvie, J.M., Herzog, E.D., Breidenbach, A., Vogler, C., Wozniak, D.F., and Sands, M.S. (2007). Development of sensory, motor and behavioral deficits in the murine model of Sanfilippo syndrome type B. PLoS One *2*, e772. https://doi.org/10.1371/journal.pone.0000772.

55. Polgreen, L.E., Chen, A.H., Pak, Y., Luzzi, A., Morales Garval, A., Acevedo, J., Bitan, G., Iacovino, M., O'Neill, C., and Eisengart, J.B. (2024). Anakinra in Sanfilippo syndrome: a phase 1/2 trial. Nat. Med. *30*, 2473–2479. https://doi.org/10.1038/s41591-024-03079-3.

56. Attar, A., Ripoli, C., Riccardi, E., Maiti, P., Li Puma, D.D., Liu, T., Hayes, J., Jones, M.R., Lichti-Kaiser, K., Yang, F., et al. (2012). Protection of primary neurons and mouse brain from Alzheimer's pathology by molecular tweezers. Brain *135*, 3735–3748. https://doi.org/10.1093/brain/aws289.

57. Malik, R., Di, J., Nair, G., Attar, A., Taylor, K., Teng, E., Klärner, F.G., Schrader, T., and Bitan, G. (2018). Using Molecular Tweezers to Remodel Abnormal Protein Self-Assembly and Inhibit the Toxicity of Amyloidogenic Proteins. Methods Mol. Biol. *1777*, 369–386. https://doi.org/10.1007/978-1-4939-7811-3_24.

58. Di, J., Siddique, I., Li, Z., Malki, G., Hornung, S., Dutta, S., Hurst, I., Ishaaya, E., Wang, A., Tu, S., et al. (2021). The molecular tweezer CLR01 improves behavioral deficits and reduces tau pathology in P301S-tau transgenic mice. Alzheimers Res. Ther. *13*, 6. https://doi.org/10.1186/s13195-020-00743-x.

59. Bengoa-Vergniory, N., Faggiani, E., Ramos-Gonzalez, P., Kirkiz, E., Connor-Robson, N., Brown, L.V., Siddique, I., Li, Z., Vingill, S., Cioroch, M., et al. (2020). CLR01 protects dopaminergic neurons *in vitro* and in mouse models of Parkinson's disease. Nat. Commun. *11*, 4885. https://doi.org/10.1038/s41467-020-18689-x.

60. Hemsley, K.M., and Hopwood, J.J. (2005). Development of motor deficits in a murine model of mucopolysaccharidosis type IIIA (MPS-IIIA). Behav. Brain Res. *158*, 191–199. https://doi.org/10.1016/j.bbr.2004.08.019.